Published in final edited form as:
Ultrasound Med Biol. 2012 March ; 38(3): 443–453. doi:10.1016/j.ultrasmedbio.2011.12.008.

DIFFERENTIATION OF BENIGN PERIABLATIONAL ENHANCEMENT FROM RESIDUAL TUMOR FOLLOWING RADIOFREQUENCY ABLATION USING CONTRAST-ENHANCED ULTRASONOGRAPHY IN A RAT SUBCUTANEOUS COLON CANCER MODEL

Hanping Wu[*], **Ravi Patel**[†], **Yuanyi Zheng**[*,‡], **Luis Solorio**[†], **Tianyi M. Krupka**[*], **Nicholas P. Ziats**[§], **John R. Hagga**[*], and **Agata A. Exner**[*]

[*]Department of Radiology, Case Western Reserve University, Cleveland, OH, USA

[†]Department of Biomedical Engineering, Case Western Reserve University, Cleveland, OH, USA

[§]Department of Pathology, Case Western Reserve University, Cleveland, OH, USA

Abstract

Benign periablational enhancement (BPE) response to thermal injury is a barrier to early detection of residual tumor in contrast enhanced imaging after radiofrequency (RF) ablation. The objective of this study was to evaluate the role of quantitative of contrast-enhanced ultrasound (CEUS) in early differentiation of BPE from residual tumor in a BD-IX rat subcutaneous colon cancer model. A phantom study was first performed to test the validity of the perfusion parameters in predicting blood flow of two US contrast imaging modes – contrast harmonic imaging (CHI) and microflow imaging (MFI). To create a simple model of BPE, a peripheral portion of the tumor was ablated along with surrounding normal tissue, leaving part of the tumor untreated. First-pass dynamic enhancement (FPDE) and MFI scans of CEUS were performed before ablation and immediately, 1, 4, and 7 days after ablation. Time-intensity-curves in regions of BPE and residual tumor were fitted to the function $y=A(1-\exp(-\beta(t-t_0))+C$, in which A, β, t_0 and C represent blood volume, flow speed, time to start and baseline intensity, respectively. In the phantom study, positive linear correlations were noted between A, β, Aβ and contrast concentration, speed, and flow rate, respectively, in both CHI and MFI. On CEUS images of the *in vivo* study, the unenhanced ablated zone was surrounded by BPE and irregular peripheral enhancement consistent with residual tumor. On days 0, 4 and 7, blood volume (A) in BPE was significantly higher than that in residual tumor in both FPDE imaging and MFI. Significantly greater blood flow (Aβ) was seen in BPE compared to residual tumor tissue in FPDE on day 7 and in MFI on day 4. The results of this study demonstrate that qualitative CEUS can be potentially used for early detection of viable tumor in post-ablation assessment.

Address correspondence to: Agata. A. Exner, Ph.D., Department of Radiology, Case Western Reserve University, 11100 Euclid Avenue, Cleveland, OH 44106. agata.exner@case.edu, Tel: 216-844-3544.
[‡]now at Ultrasound Department, Second Affiliated Hospital of Chongqing Medical University, Chongqing, P.R. China

Keywords

Radiofrequency ablation; Post ablation assessment; Contrast-enhanced ultrasound; First-pass dynamic enhancement; Microflow imaging

INTRODUCTION

Radiofrequency (RF) ablation has become one of the most frequently utilized interventions in the management of unresectable tumors (Gazelle et al. 2004; Machi et al. 2006; Joosten and Ruers 2007; Park et al. 2008) but local recurrence rates at the treatment site have been reported to be as high as 12% (McWilliams et al. 2010). Radiologic follow-up techniques capable of detecting residual or recurrent tumor soon after the intervention are, therefore, an essential component of the management process. However, early detection of residual or recurrent disease on follow-up imaging using common anatomic imaging techniques, such as CT or MRI, has proven to be challenging. The accuracy of assessment is often limited because of the presence of an ablation-induced hyperemic rim around the margin of ablated tissue which is referred to as benign periablational enhancement (BPE) as recommended by the International Working Group on Image-Guided Tumor Ablation (Goldberg et al. 2009). BPE can be seen immediately after thermal ablation and remains for 2–6 months (Lencioni et al. 2001; Lim et al. 2001; Lu et al. 2005; Solbiati and Arsizio 2007; Kuehl et al. 2008; Rutherford et al. 2008). Previous clinical imaging and pathology correlation studies showed that the BPE is usually uniform in thickness. In contrast, viable residual or recurrent tumor shows focal irregular peripheral rim enhancement on contrast enhanced CT or MR images (Goldberg et al. 2000; Hsu et al. 2005) but detecting viable tumor at early time points after treatment based solely on these morphological findings can be difficult. According to one review, the inflammatory response "…is impossible to distinguish from a rim of vascularized residual tumor" (Curley 2003). Dromain et al., reported that CT and MR imaging may depict tumor recurrence at 4 months after RF ablation at the earliest since the BPE disappeared over time and was present in only 8% of the RF-ablated areas after this time interval (Dromain et al. 2002). The overall sensitivity to detect residual tumor after RF ablation when assessed with CT or MRI ranges between 44% and 89% (Lim et al. 2001; Dromain et al. 2002; Blokhuis et al. 2004). Since early detection of residual tumor allows initiation of additional treatment with potential benefits for patient survival (Curley 2001; Izzo et al. 2001; Veit et al. 2006), improved or novel imaging methods are needed for early detection of residual tumor and accurate follow-up of local tumor ablation.

One possible solution may be found is using the latest generation of ultrasound (US) contrast agents and related imaging technologies, such as contrast sequence imaging, contrast harmonic imaging (CHI), etc. These techniques allow continuous, real-time imaging of contrast enhancement with higher temporal resolution than CT or MRI. Moreover, these new techniques have been recently used for tumor detection, guidance of tumor ablation and to evaluate post RF ablation both in animal studies and clinical studies with promising results (Solbiati et al. 2004; Chen et al. 2007; Lu et al. 2007; Bartolotta et al. 2008). However as in contrast enhanced CT or MR, peripheral reactive hyperemia following RF ablation treatment can also be seen on CEUS, and this might confuse the evaluation of residual tumor (Vogt et al. 2007; Hoeffel et al. 2010). In previous studies, differences between BPE and residual tumor were evaluated by qualitative visual inspection, and early differentiation of residual tumor (within 1 month after RF ablation) from inflammatory tissue was still problematic. One study by Vilana et al., reported that the sensitivity of contrast-enhanced US (CEUS) detection of residual hepatocellular carcinoma 24 hours after ablative treatment was 27.3% (Vilana et al. 2006).

US contrast enhanced microflow imaging (MFI) was recently introduced to better visualize tumor vasculature. MFI is an image processing method based on maximum intensity projection (MIP), also called max-hold processing. This method uses a destruction-replenishment technique, which consists of transmitting a time-sequence of ultrasound waves at a high mechanical index (MI) to destroy microbubbles in the scan plane, and then imaging the subsequent microbubble replenishment at low MI with MIP (Kamiyama 2004). This reveals tumor microvasculature which can be helpful in differentiating benign from malignant hepatic lesions (Hotta et al. 2005) and for detecting prostatic lesions in order to guide biopsies (Linden et al. 2007). To the best of our knowledge, this technique has not been previously utilized in the post-ablation assessment.

Quantitative CEUS has recently been used to explore tumor perfusion by using different mathematical models to fit the time-intensity-curves of lesion contrast enhancement. The proposed parameters derived from these models can be used as early indicators of tumor diagnosis and treatment response evaluation, such as in antiangiogenic therapy (Guibal et al. 2010). We hypothesize that quantitative CEUS could be more sensitive in differentiation of residual tumor from BPE in the post-ablation assessment than conventional CEUS imaging. In the current study, we first designed a phantom study to test the validity of the perfusion parameters of a mono-exponential model in predicting the blood flow with CHI and MFI. We then created a partially ablated tumor model, and tested the possibility of differentiation of residual tumor from the BPE following RF ablation by CEUS using quantification of first-pass dynamic enhancement (FPDE) and MFI, in hopes that differences in perfusion would lead to an effective means of differentiating these regions in ablation follow-up.

MATERIALS AND METHODS

Preparation of Ultrasound Contrast Agents

The lipid shells of microbubbles were composed of 1, 2-Dipalmitoyl-sn-Glycero-3-Phosphocholine (DPPC), 1, 2-Dipalmitoyl-sn-Glycero-3-Phosphoethanolamine (DPPE), and 1, 2-Dipalmitoyl-sn-Glycero-3-Phosphate (DPPA) (Avanti Polar Lipids, Inc.; Alabaster, AL) with a mass ratio of 5:2:1. The lipid mixture was dissolved in chloroform and dried for two hours under a hood. Glycerol (Sigma-Aldrich Corp.; St. Louis, MO) and phosphate buffered saline (pH 7.0, Sigma-Aldrich Corp.; St. Louis, MO) were then added to the dried lipids and incubated at 37°C for 30 min. An aliquot of the solution was then transferred into gas-tight vials into which perfluoropropane gas (C_3F_8) was added. Microbubbles were formed using a VialMix mixing machine (DuPont Pharma Co., Billerica, MA) to mechanically agitate the solution for 45 s. The morphology of the resulting microbubbles was determined using an optical microscope (Carl Zeiss Achroplan 100, NA 1.0; Thornwood, NY) and the diameter was measured with 90plus Particle Size Analyzer (Brookhaven Instruments Corporation, NY). The diameter of the bubbles was approximately 1 μm. The details of microbubble preparation and size measurement were reported in our previous paper (Krupka et al. 2010).

In Vitro Phantom Study

Setup of the phantom study is shown in Fig 1a. To make this phantom, a plastic tube (0.74 mm outside diameter) was used to form a channel in 2% agarose gel. After cooling and setting of the agarose gel, the tube was removed and each side of the channel was connected with a 200 μl pipette tip. The phantom was then infused with microbubble solution at different dilution factors in normal saline (1:250, 1:1250, 1:6250, and 1:31250) at eight constant flow rates using an infusion pump. The calculated flow speed ranged from 0.73 mm/s to 72.8 mm/s. US scans were performed with an Aplio™ SSA-770A Ultrasound system (Toshiba Medical Imaging Systems, Tokyo, Japan) using a 10MHz linear transducer.

The transducer was immobilized using a clamp and aligned longitudinally with the phantom vessel (Fig 1b). 60s perfusion images of CHI and MFI with flash replenishment every 20 seconds were acquired with the following settings: CHI frequency, H6.6 (MHz); mechanical index (MI), 0.1; imaging frame rate, 45 fps; dynamic range, 90 dB; 2D gain, 80 dB. Both CHI and MFI sequence of images were exported as AVI clips (Codec, MPEG-4 V2; video frame rate, 15 fps; image quality, low) for off-line data processing. A typical time-gray intensity-curve of a ROI in the vessel phantom is shown in Fig 1c.

Animal Model

A well-established rat tumor model, DHD/K12/TRb adenocarcinoma was used in this study (Krupka et al. 2007). The experimental protocols were approved by the Institutional Animal Care and Use Committee at our institution. Anesthesia was conducted with 3% isoflurane in oxygen (1 L/min) via a vaporizer (EZ150 Isoflurane Vaporizer, EZ Anesthesia™). The DHD/K12/TRb cell line, originating from a 1, 2-dimethylhydrazine-induced colon adenocarcinoma in BDIX rats, was cultured in RPMI-1640 media with 10% fetal bovine serum and passaged weekly. Eight six-week-old male BDIX rats (body weight 150–180g, purchased from Charles River Laboratories Inc., Wilmington, MA) were used for inoculation. Tumors were inoculated subcutaneously with a bilateral injection of 0.05 mL cell suspension (2×10^6 cells/mL) on the thigh using a 26-gauge needle. Five weeks later, the tumors were used for this study, and the maximum tumor diameter ranged from 0.5–0.9 cm.

Initiation of Inflammatory Response by RF Ablation

RF ablation was performed by using a 500 kHz RF generator (Radionics, Cool-tip RF system, Radionics Inc., Burlington, MA) and a custom-designed 21-gauge monopolar needle electrode. Here, the 21G disposable hypodermic needle was used as a RF antenna covered with a Teflon tube with the 0.5 cm tip exposed, and a thermocouple located in the central core of the needle to monitor temperature during ablation. A grounding pad was placed on the abdomen, and US gel was used to ensure proper contact. To create a simple model of BPE only the peripheral portion of the tumor was ablated along with surrounding normal tissue, leaving part of the tumor untreated. To carry out the ablation the electrode was inserted at a depth of 0.5 cm, and tumors were treated to a temperature of 80°C ± 2 for 3 min at 1–2W. Preliminary studies showed that this setting could obtain a proximal 0.5cm ablated zone in diameter, thereby ablating part of the tumor and adjacent normal tissue.

US Imaging Protocol

US scans were obtained before RF ablation, immediately post treatment (within 10 minutes) and 1, 4, 7 days after RF ablation with the same US system and transducer by two radiologists (H.W. and Y.Z., with 10 and 9 years of experience in ultrasound imaging, respectively). The transducer was immobilized using a clamp, and the rat thigh was laid supine on the probe with a custom designed gel mold. The position of the tumor was adjusted so that the field of view included the ablated region, residual viable tumor and normal muscle with a 2D Doppler scan. A solution of 0.05 mL of contrast was injected as a bolus via the tail vein and flushed with 0.5 mL normal saline. The first 60 s of first-pass dynamic enhancement (FPDE) images after contrast administration were acquired using the contrast harmonic imaging (CHI) mode with the following imaging settings: CHI frequency, H6.6 (MHz); Mechanical index (MI), 0.1; imaging frame rate, 45 fps; dynamic range, 90 dB; 2D gain, 80 dB. Then the scan mode was switched to MFI with the same imaging settings to acquire a series of destruction-replenishment images with 10 s duration. Both FDPE and MFI sequence of images were exported as AVI clips. The time interval between pre-ablation and immediate post-ablation CEUS scans was 30 minutes to allow complete microbubble clearance.

Imaging Analysis

The AVI clips of CEUS scans were transferred to a PC, and the data was imported into ImageJ 1.42 for analysis. In the phantom study, a rectangular ROI was set in the center of the tubing (Fig 1c). In the *in vivo* study, since only part of the tumor was ablated, BPE (located at the distal side of unenhanced ablated zone) and residual tumor (located at the proximal part of the tumor) could be accurately discerned on enhanced FPDE and MFI images. A crescent shaped ROI was drawn in the BPE or residual tumor on FDPE image with the consent of 2 authors (H.W. and Y.Z.). Representative ROI selection is shown in Fig 2(a–c). Here, the ROI of BPE covers most of the enhanced part of the hyperemic rim of the ablated region. The residual tumor is composed of a less enhanced inner core and a more enhanced peripheral zone. The ROI of residual tumor was positioned in the more enhanced peripheral zone. The locations of ROIs on MFI images were identical to the corresponding FDPE images at each time point. The mean time-video-intensity of each ROI was then calculated and then imported into Matlab for further analysis using a custom algorithm. Since the linearized signal intensity (SI_{linear}) is proportional to contrast concentration (Arditi et al. 2006), the video intensity data was converted to SI_{linear} as previously described (Guibal et al. 2010). Briefly, the video intensity data was first converted to SI in decibels (SI_{dB}) by using the grayscale bar. Then, the SI_{linear} was calculated by using the reverting log-compression law: $SI_{\text{linear}} = 10^{(SI\text{dB}/10)}$. The time-$SI_{\text{linear}}$ curves were then fit with an mono-exponential function (Wei et al. 1998): $y=A(1-\exp(-\beta(t-t_0)))+C$, where y is the perfusion model function, A is the plateau value as an estimate of the regional blood volume, β is the replenishment rate as an estimate of microbubble velocity, t_0 is the delay, C is the baseline and Aβ is an estimate of flow. In some experimental FPDE data, a decay of signal intensity was encountered after the peak. In these cases, the data was truncated to 10 sec after peak signal intensity was reached. A typical example of FPDE and MFI curve fitting outputs is shown in Fig 2d and 2e.

Histopathologic Examination

Animals were euthanized on day 7 following treatment. Tumor and ablated tissue were dissected and sectioned at an orientation corresponding to the plane of the ultrasound image. The tissue was fixed in 10% formalin solution and embedded in paraffin. Slides of 5 μm thickness were cut and stained with hematoxylin and eosin (H&E). All histological processing was carried out by the Histology Core Facility of the Case Comprehensive Cancer Center. Histopathologic examination of the tumors was conducted by analysis blinded to the US findings (Carl Zeiss Achroplan 100, NA 1.0; Thornwood, NY). The locations of the ablated region, the BPE and residual tumor on US images were verified by histology findings with the consensus opinion of a pathologist (N.P.Z).

Statistical Analysis

All data was presented as mean ± standard deviation (SD). In the phantom study, linear correlation coefficients between perfusion parameters and bubble concentration, speed and the product of concentration and speed were calculated. In the *in vivo* study, at each observation time point the values of perfusion parameters of two ROIs were compared with the Wilcoxon Signed-Rank test. Statistical analyses were performed with VassarStat online.

RESULTS

In vitro phantom study

In these experiments, the parameters A, β and Aβ in the mono-exponential function correspond to the microbubble concentration (C), infusion speed (S) and flow rate (product of C and S). Results of in vitro phantom validation are shown in Fig 3. Fig 3a shows the

correlations between A and C at high (72.8 mm/sec), medium (41.7 mm/sec) and low speeds (8.5 mm/sec). Fig 3b shows the correlations between β and S at the highest (1:250 dilution) and lowest bubble concentrations (1:31250 dilution). Fig 3c shows the correlations between Aβ and $C*S$ in lumped data. In both CHI and MFI modes, positive linear correlations were noted between A, β, Aβ and C, S, $C*$S respectively ($r > 0.91$). At every flow condition, the parameters A, β and Aβ calculated with CHI were greater than those with MFI, but the relative changes were consistent between the two imaging modes.

In vivo analysis

FPDE and MFI at peak enhancement of a representative tumor before RF ablation, immediately following (day 0) and 1, 4, 7 days after RF ablation are shown in Fig 4. Before ablation, the overall tumor enhancement varied based on the extent of central necrosis, yet the border between the tumor and non-tumor regions was distinct due to tumor rim enhancement. Immediately following ablation the treated ablation zone did not show enhancement. A homogenous rim enhancement (BPE) in muscle adjacent to the ablation zone indicated a hyperemic rim induced by ablative treatment. Additionally, nodular enhancing abnormalities were noted in the residual tumor zone, which showed a heterogeneous enhancing core with an enhanced rim. A distinct boundary was noted by visual inspection between the unenhanced coagulation zone and the surrounding hyperemic rim or residual tumor. However, from day 1 to 7 after ablation, this boundary became increasingly difficult to discern, as the width of the hyperemic inflammatory rim increased and the size of unenhanced region decreased. This effect was particularly pronounced on day 7. In all of these time points, MFI showed the boundaries between the enhanced and non-enhanced regions more clearly than FPDE.

In addition to qualitative visual examination, differences in signal echogenicity between BPE and residual tumor were also quantified as described above. Changes in blood volume (A), flow velocity (β), and blood flow (Aβ) values in BPE and residual tumor regions on FPDE and MFI are shown in Fig 5 and Tables 1–2. With FPDE imaging, a greater blood volume (A) in BPE compared to that in residual tumor was noted in 7/8, 5/8, 7/8 and 7/8 tumors on days 0, 1, 4, and 7, respectively. With MFI, a greater blood volume in BPE compared to that in residual tumor was noted in 6/8, 4/8, 8/8 and 7/8 tumors on days 0, 1, 4, and 7, respectively. The mean value of blood volume calculated using both FPDE and MFI in BPE was significantly higher ($p<0.05$) than that in residual tumor on 0, 4 and 7 days after ablation.

A higher blood flow (Aβ) in BPE compared to that in residual tumor was noted in 5/8, 6/8, 4/8, 7/8 tumors with FPDE imaging, and in 3/8, 4/8, 6/8, 6/8 tumors with MFI on days 0, 1, 4, 7, respectively. However, the difference in blood flow was significant ($p<0.05$) only on day 7 on FPDE and on day 4 on MFI. The difference in flow speed (β) in BPE and residual tumor was not significant except on day 7 in FPDE where the former is significantly higher than the latter.

Histological examination of tissue one week after ablation showed extensive coagulation necrosis and granulation tissue with microvasculature at the boundary of the ablation zone. Central necrosis was noted in the residual tumor, and numerous lymphocytes were seen in the fibrous capsule of the residual viable tumor (Fig 6).

DISCUSSION

CEUS is used as a new modality to explore perfusion in cardiac muscle, tumor, and liver tissue. The replenishing contrast enhancement curves of harmonic imaging or phase-inverse imaging when microbubbles are homogenously distributed in blood pool fitted with a mono-

exponential function $y=A(1-\exp(-\beta t))$ is a standard method to calculate the flow parameters – A, β and Aβ (Quaia 2007). MFI is a relatively new technique of highlighting microvasculature. By combining a flash-replenishment (FR) sequence and max-hold processing (Quaia 2007), MFI has been shown to be an excellent tool for revealing the vascular network of lesions (Yang et al. 2007; Du et al. 2008). In this imaging procedure, the FR sequence destroys all bubbles in the imaging plane using a burst scan at high MI. Subsequently, during the bubble replenish phase, the maximum bubble intensity at each location is collected and stored until a higher intensity signal at the same location is reached. Then, this higher signal intensity is registered and replaces the previous value using max-hold processing. Along with good microvessel display, MFI has the advantage of repetitive trials within an injection. These repeated trials make it easy to change scan planes and improve the post-ablation assessment imaging. MFI has not been used in qualification of blood flow in CEUS. The phantom study in this experiment noted that A, β and Aβ in both CHI and MFI modes were proportional to contrast concentration, speed and flow rate, respectively. Furthermore, *in vivo* our fitting results confirmed that both FPDE and replenishing MFI time-signal intensity curves obey this mono-exponential function, and MFI demarcated the boundaries between the enhanced and non-enhanced region more clearly than FPDE. These suggest that MFI could be used in qualification of flow in CEUS as well.

In this study, we designed a small rodent model to mimic the residual tumor and BPE after RF ablation and overcome the aforementioned problems. In the current model, subcutaneous colorectal tumors were inoculated, and an adjacent hyperemic rim was intentionally induced by ablating normal muscle in addition to half of the tumor. Part of each tumor remained viable and was used to simulate a situation where a residual tumor may remain after ablation. There are several advantages to using this model. First, we can be certain that no residual tumor was located within the hyperemic rim. This is useful to examine and distinguish the underlying differences between tumor tissue and the hyperemic rim. Second, this model is especially beneficial for the study of arterial phase tumor perfusion, since there is no interference from the portal vein. This allows us to have a better understanding of the perfusion before moving on to a more complex, clinically relevant model, such as hepatocellular carcinoma. Finally, motion artifacts due to respiration can be avoided because of the remote location of the tumor.

Using this subcutaneous tumor model, the current study explored changes in the perfusion profiles of BPE and residual tumor using FPDE and MFI of CEUS examination at different time points up to 1 week after RF ablation. We found enhancement surrounding the coagulation zone, which included BPE and nodular enhancing abnormalities and a distinct border between an unenhanced coagulation zone and surrounding enhanced tissue immediately after ablation with harmonic CEUS imaging. However, this border became less distinct over time. This is most likely due to the typical inflammatory response and granulation tissue formation after RF ablation (Wu et al. 2009). However, it was difficult to differentiate BPE from residual tumor by visual judgment alone due to contrast enhancement in both regions.

In order to differentiate viable residual tumor from BPE, we analyzed the difference of perfusion parameters (blood volume, speed and blood flow) in these 2 regions. Our data showed that a significantly higher blood volume in BPE was noted on days 0, 4 and 7 when compared with the blood volume in residual tumor with both FPDE and MFI. A similar difference was seen in blood flow (Aβ); however, the differences were significant only on day 7 in FPDE imaging and on day 4 in MFI. No obvious difference in flow speed was noted in these regions except on day 7 with FPDE imaging. These differences suggest that blood volume might be the most sensitive parameter to use in order to differentiate residual

tumor from BPE in post-ablation assessment using CEUS. The histology analysis on day 7 showed coagulation in the ablated region, granulation tissue at the boundary of the ablation zone (normal tissue but not the residual tumor) and the formation of a fibrous capsule with some small vessels in the vicinity of the residual viable tumor. These suggest that higher blood volume and blood flow in the hyperemic rim of the ablated zone than in the residual tumor on days 4 and 7 may most likely be due to more vasculature in inflammatory tissue than in residual tumor in this particular tumor model after ablation. Immediately after ablation, higher perfusion in BPE might be due to the vessel dilation in response to heat (Emami et al. 1980).

The changes in perfusion parameters at different time points after ablation reflect the pathophysiological changes in the ablated tissue, surrounding normal tissue and residual tumor. We found blood volume and blood flow in BPE decreased on day 1 and increased on days 4 and 7 after ablation. Histology changes in the same tumor model on days 2 and 7 after RF ablation were reported in our previous study (Wu et al. 2009). In short, the peripheral rim of ablated tumor presented with a hyperemic reaction with dilated vessels and congestion on day 2 after ablation and numerous inflammatory vessels and granulation tissue formation on day 7. Based on these post-ablation histological findings, it is possible that on day 1, a blood hypercoagulable state or thrombosis caused by endothelial cell damage leads to congestion and decreased blood perfusion. However, on days 4 and 7, the process of granulation tissue formation will increase the perfusion.

There are several limitations to this study. First, parameter A and Aβ calculation requires post-acquisition image processing and data analysis techniques, as the small difference between these parameters in hyperemic rim and viable tumor rim might not be discerned by simple viewing of the video clips. Although some ultrasound scanners are equipped with a perfusion analysis package, which can fit the perfusion curve and calculate the parameter immediately after examination, we opted to use ImageJ and created a Matlab code to analyze the offline videos although the algorithm is similar to the vendor software. Second, there may be a difference in the perfusion in BPE and residual tumor after ablation in different tumor species and organs due to a different microvasculature profile. For example, Kim TJ, et al reported MR perfusion analysis using a blood pool contrast agent permitted accurate differentiation of BPE from residual tumor in a rabbit muscle VX2 carcinoma model after ablation. However, the enhancement in residual tumor was significantly higher than that in BPE and the microvessel density in residual tumor was significantly higher than that in BPE as well in this tumor model (Kim et al. 2005). In our study, histology showed that more vessels were found in BPE than residual tumor on day 7 after ablation. We assumed that the MVD in BPE was higher than that in residual tumor on days 0 and 4 after ablation. The findings of Kim's study and our study indicate that both MR perfusion and US perfusion can be used to characterize vasculature, and applied to differentiate BPE from residual or recurrent tumor. However, it is possible that the difference between BPE and residual tumor may be tumor specific and may not be perceptible in all tumor types, which may limit the broader application of this technique. Furthermore, since liver and kidney tumors are more clinically relevant in RF ablation treatment than subcutaneous tumor, our technique needs to undergo further testing in the renal tumor model which has extremely high cortical blood flow, and the liver tumor model which should account for portal vein perfusion.

CONCLUSION

In this study, we explored the differences in perfusion values of FPDE and MFI in BPE and residual tumor after RF ablation in order ascertain whether quantitative CEUS can be used to differentiate viable tumor from BPE after tumor thermal ablation. Our results demonstrate

that it is indeed able to detect early differences in the various ablation zones and that blood volume may be the most sensitive parameter for this evaluation. If sufficiently refined and demonstrated in clinical practice, this technique may lead to improved follow-up after interventional oncology procedures.

Acknowledgments

The authors are grateful for the partial support of the National Institutes of Health (R01CA136857, R21CA131014 and 5P30043703).

References

Arditi M, Frinking PJ, Zhou X, Rognin NG. A new formalism for the quantification of tissue perfusion by the destruction-replenishment method in contrast ultrasound imaging. IEEE Trans Ultrason Ferroelectr Freq Control. 2006; 53:1118–29. [PubMed: 16846144]

Bartolotta TV, Taibbi A, Midiri M, De Maria M. Hepatocellular cancer response to radiofrequency tumor ablation: contrast-enhanced ultrasound. Abdom Imaging. 2008; 33:501–11. [PubMed: 17786507]

Blokhuis TJ, van der Schaaf MC, van den Tol MP, Comans EF, Manoliu RA, van der Sijp JR. Results of radio frequency ablation of primary and secondary liver tumors: long-term follow-up with computed tomography and positron emission tomography-18F-deoxyfluoroglucose scanning. Scand J Gastroenterol Suppl. 2004:93–7. [PubMed: 15696856]

Chen MH, Wu W, Yang W, Dai Y, Gao W, Yin SS, Yan K. The use of contrast-enhanced ultrasonography in the selection of patients with hepatocellular carcinoma for radio frequency ablation therapy. J Ultrasound Med. 2007; 26:1055–63. [PubMed: 17646367]

Curley SA. Radiofrequency ablation of malignant liver tumors. Oncologist. 2001; 6:14–23. [PubMed: 11161225]

Curley SA. Radiofrequency ablation of malignant liver tumors. Ann Surg Oncol. 2003; 10:338–47. [PubMed: 12734080]

Dromain C, de Baere T, Elias D, Kuoch V, Ducreux M, Boige V, Petrow P, Roche A, Sigal R. Hepatic tumors treated with percutaneous radio-frequency ablation: CT and MR imaging follow-up. Radiology. 2002; 223:255–62. [PubMed: 11930075]

Du J, Li FH, Fang H, Xia JG, Zhu CX. Microvascular architecture of breast lesions: evaluation with contrast-enhanced ultrasonographic micro flow imaging. J Ultrasound Med. 2008; 27:833–42. [PubMed: 18499843]

Emami B, Nussbaum GH, TenHaken RK, Hughes WL. Physiological effects of hyperthermia: response of capillary blood flow and structure to local tumor heating. Radiology. 1980; 137:805–9. [PubMed: 7444065]

Gazelle GS, McMahon PM, Beinfeld MT, Halpern EF, Weinstein MC. Metastatic colorectal carcinoma: cost-effectiveness of percutaneous radiofrequency ablation versus that of hepatic resection. Radiology. 2004; 233:729–39. [PubMed: 15564408]

Goldberg SN, Gazelle GS, Compton CC, Mueller PR, Tanabe KK. Treatment of intrahepatic malignancy with radiofrequency ablation: radiologic-pathologic correlation. Cancer. 2000; 88:2452–63. [PubMed: 10861420]

Goldberg SN, Grassi CJ, Cardella JF, Charboneau JW, Dodd GD 3rd, Dupuy DE, Gervais DA, Gillams AR, Kane RA, Lee FT Jr, Livraghi T, McGahan J, Phillips DA, Rhim H, Silverman SG, Solbiati L, Vogl TJ, Wood BJ, Vedantham S, Sacks D. Image-guided tumor ablation: standardization of terminology and reporting criteria. J Vasc Interv Radiol. 2009; 20:S377–90. [PubMed: 19560026]

Guibal A, Taillade L, Mule S, Comperat E, Badachi Y, Golmard JL, Le Guillou-Buffello D, Rixe O, Bridal SL, Lucidarme O. Noninvasive contrast-enhanced US quantitative assessment of tumor microcirculation in a murine model: effect of discontinuing anti-VEGF therapy. Radiology. 2010; 254:420–9. [PubMed: 20093514]

Hoeffel C, Pousset M, Timsit MO, Elie C, Mejean A, Merran S, Tranquart F, Khairoune A, Joly D, Richard S, Helenon O, Correas JM. Radiofrequency ablation of renal tumours: diagnostic accuracy

of contrast-enhanced ultrasound for early detection of residual tumour. Eur Radiol. 2010; 20:1812–21. [PubMed: 20204642]

Hotta N, Tagaya T, Maeno T, Ayada M, Sato K, Ishikawa T, Okumura A, Fukuzawa Y, Kakumu S. Advanced dynamic flow imaging with contrast-enhanced ultrasonography for the evaluation of tumor vascularity in liver tumors. Clin Imaging. 2005; 29:34–41. [PubMed: 15859016]

Hsu CP, Razavi MK, So SK, Parachikov IH, Benaron DA. Liver tumor gross margin identification and ablation monitoring during liver radiofrequency treatment. J Vasc Interv Radiol. 2005; 16:1473–8. [PubMed: 16319153]

Izzo F, Barnett CC Jr, Curley SA. Radiofrequency ablation of primary and metastatic malignant liver tumors. Adv Surg. 2001; 35:225–50. [PubMed: 11579813]

Joosten J, Ruers T. Local radiofrequency ablation techniques for liver metastases of colorectal cancer. Crit Rev Oncol Hematol. 2007; 62:153–63. [PubMed: 17317204]

Kamiyama N. Update of ultrasound contrast imaging. International Congress Series. 2004; 1274:53–6.

Kim TJ, Moon WK, Cha JH, Goo JM, Lee KH, Kim KH, Lee JW, Han JG, Weinmann HJ, Chang KH. VX2 carcinoma in rabbits after radiofrequency ablation: comparison of MR contrast agents for help in differentiating benign periablational enhancement from residual tumor. Radiology. 2005; 234:423–30. [PubMed: 15591437]

Krupka TM, Solorio L, Wilson RE, Wu H, Azar N, Exner AA. Formulation and characterization of echogenic lipid-Pluronic nanobubbles. Mol Pharm. 2010; 7:49–59. [PubMed: 19957968]

Krupka TM, Weinberg BD, Wu H, Ziats NP, Exner AA. Effect of intratumoral injection of carboplatin combined with pluronic P85 or L61 on experimental colorectal carcinoma in rats. Exp Biol Med (Maywood). 2007; 232:950–7. [PubMed: 17609512]

Kuehl H, Antoch G, Stergar H, Veit-Haibach P, Rosenbaum-Krumme S, Vogt F, Frilling A, Barkhausen J, Bockisch A. Comparison of FDG-PET, PET/CT and MRI for follow-up of colorectal liver metastases treated with radiofrequency ablation: initial results. Eur J Radiol. 2008; 67:362–71. [PubMed: 18155866]

Lencioni R, Cioni D, Bartolozzi C. Percutaneous radiofrequency thermal ablation of liver malignancies: techniques, indications, imaging findings, and clinical results. Abdom Imaging. 2001; 26:345–60. [PubMed: 11441546]

Lim HK, Choi D, Lee WJ, Kim SH, Lee SJ, Jang HJ, Lee JH, Lim JH, Choo IW. Hepatocellular carcinoma treated with percutaneous radio-frequency ablation: evaluation with follow-up multiphase helical CT. Radiology. 2001; 221:447–54. [PubMed: 11687689]

Linden RA, Trabulsi EJ, Forsberg F, Gittens PR, Gomella LG, Halpern EJ. Contrast enhanced ultrasound flash replenishment method for directed prostate biopsies. J Urol. 2007; 178:2354–8. [PubMed: 17936814]

Lu DS, Yu NC, Raman SS, Limanond P, Lassman C, Murray K, Tong MJ, Amado RG, Busuttil RW. Radiofrequency ablation of hepatocellular carcinoma: treatment success as defined by histologic examination of the explanted liver. Radiology. 2005; 234:954–60. [PubMed: 15681691]

Lu MD, Yu XL, Li AH, Jiang TA, Chen MH, Zhao BZ, Zhou XD, Wang JR. Comparison of contrast enhanced ultrasound and contrast enhanced CT or MRI in monitoring percutaneous thermal ablation procedure in patients with hepatocellular carcinoma: a multi-center study in China. Ultrasound Med Biol. 2007; 33:1736–49. [PubMed: 17629608]

Machi J, Oishi AJ, Sumida K, Sakamoto K, Furumoto NL, Oishi RH, Kylstra JW. Long-term outcome of radiofrequency ablation for unresectable liver metastases from colorectal cancer: evaluation of prognostic factors and effectiveness in first- and second-line management. Cancer J. 2006; 12:318–26. [PubMed: 16925977]

McWilliams JP, Yamamoto S, Raman SS, Loh CT, Lee EW, Liu DM, Kee ST. Percutaneous ablation of hepatocellular carcinoma: current status. J Vasc Interv Radiol. 2010; 21:S204–13. [PubMed: 20656230]

Park IJ, Kim HC, Yu CS, Kim PN, Won HJ, Kim JC. Radiofrequency ablation for metachronous liver metastasis from colorectal cancer after curative surgery. Ann Surg Oncol. 2008; 15:227–32. [PubMed: 17882491]

Quaia E. Microbubble ultrasound contrast agents: an update. Eur Radiol. 2007; 17:1995–2008. [PubMed: 17351779]

Rutherford EE, Cast JE, Breen DJ. Immediate and long-term CT appearances following radiofrequency ablation of renal tumours. Clin Radiol. 2008; 63:220–30. [PubMed: 18194700]

Solbiati, L.; Arsizio, B. CEUS for RFA Guidance and Monitoring of Therapy. RSNA 2007 93rd Scientific Assembly and Annual Meeting; 2007. p. 202

Solbiati L, Ierace T, Tonolini M, Cova L. Guidance and monitoring of radiofrequency liver tumor ablation with contrast-enhanced ultrasound. Eur J Radiol. 2004; 51 (Suppl):S19–23. [PubMed: 15311434]

Veit P, Antoch G, Stergar H, Bockisch A, Forsting M, Kuehl H. Detection of residual tumor after radiofrequency ablation of liver metastasis with dual-modality PET/CT: initial results. Eur Radiol. 2006; 16:80–7. [PubMed: 15868122]

Vilana R, Bianchi L, Varela M, Nicolau C, Sanchez M, Ayuso C, Garcia M, Sala M, Llovet JM, Bruix J, Bru C. Is microbubble-enhanced ultrasonography sufficient for assessment of response to percutaneous treatment in patients with early hepatocellular carcinoma? Eur Radiol. 2006; 16:2454–62. [PubMed: 16710666]

Vogt FM, Antoch G, Veit P, Freudenberg LS, Blechschmid N, Diersch O, Bockisch A, Barkhausen J, Kuehl H. Morphologic and functional changes in nontumorous liver tissue after radiofrequency ablation in an in vivo model: comparison of 18F-FDG PET/CT, MRI, ultrasound, and CT. J Nucl Med. 2007; 48:1836–44. [PubMed: 17942811]

Wei K, Jayaweera AR, Firoozan S, Linka A, Skyba DM, Kaul S. Quantification of myocardial blood flow with ultrasound-induced destruction of microbubbles administered as a constant venous infusion. Circulation. 1998; 97:473–83. [PubMed: 9490243]

Wu H, Exner AA, Krupka TM, Weinberg BD, Patel R, Haaga JR. Radiofrequency ablation: post-ablation assessment using CT perfusion with pharmacological modulation in a rat subcutaneous tumor model. Acad Radiol. 2009; 16:321–31. [PubMed: 19201361]

Yang H, Liu GJ, Lu MD, Xu HX, Xie XY. Evaluation of the vascular architecture of hepatocellular carcinoma by micro flow imaging: pathologic correlation. J Ultrasound Med. 2007; 26:461–7. [PubMed: 17384043]

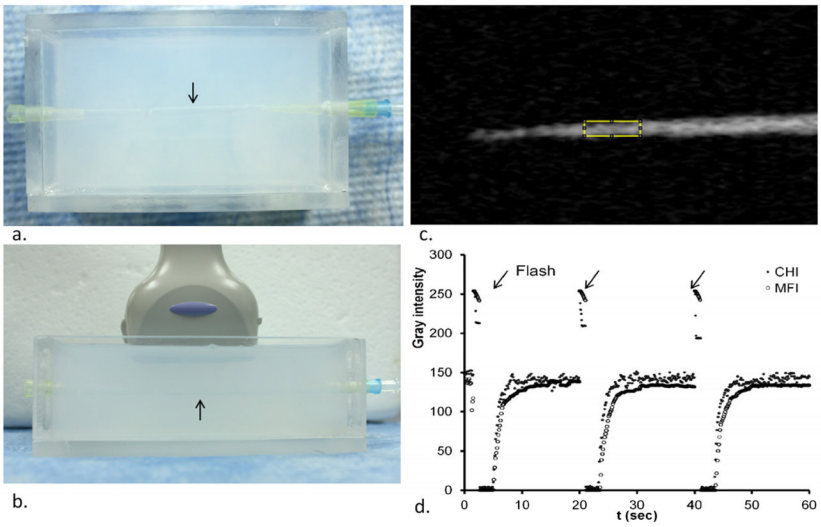

Fig. 1.

In vitro vessel phantom study. (a) Top view of a wall-less vessel phantom (arrow) made with 2% agarose gel. (b) US probe placement longitudinally to the wall-less vessel phantom (arrow). (c) Contrast harmonic image (CHI) of the phantom with microbubble solution flowing through. (d) Time- intensity curves of CHI and MFI with destruction of microbubbles (flash, arrow) every 20 seconds.

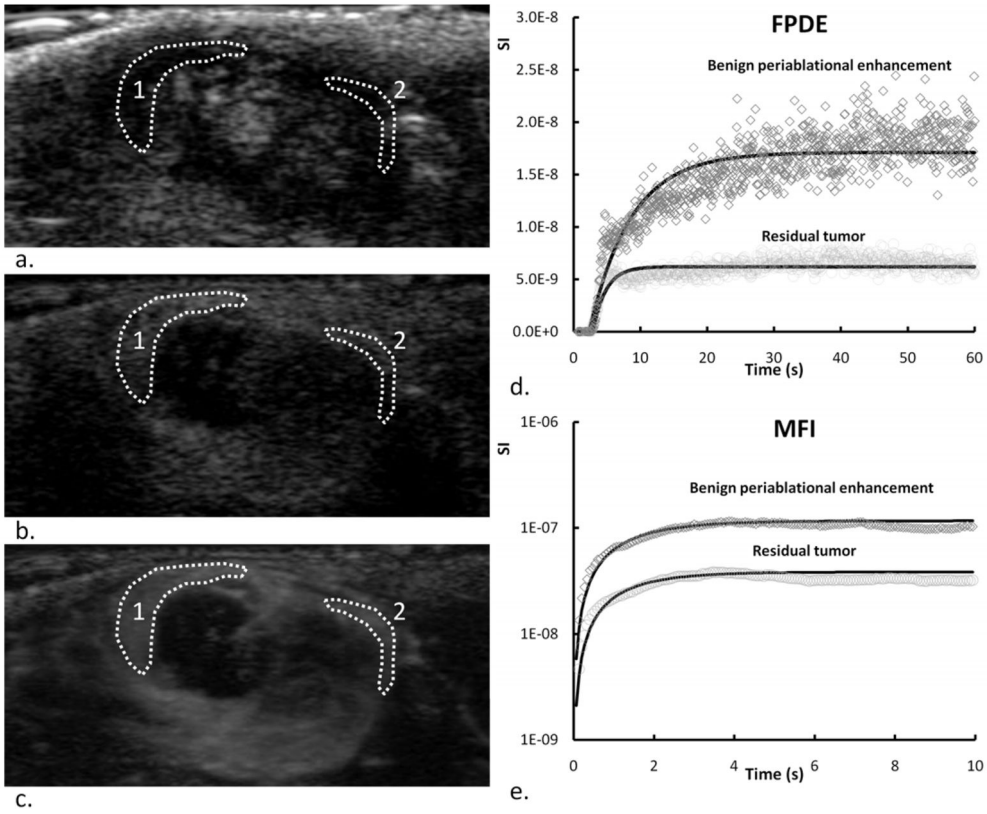

Fig. 2.

2D US (a), FPDE (b) at peak enhancement and MFI (c) images at 40 s after injection of a representative tumor on day 4 after RF ablation. ROIs in BPE (1) and residual tumor (2) were drawn manually. Contrast uptake kinetics of the first pass dynamic enhancement and of the MFI processing in the two ROIs (d, e). Corresponding fitted curves using a mono-exponential perfusion model are shown on the same plots.

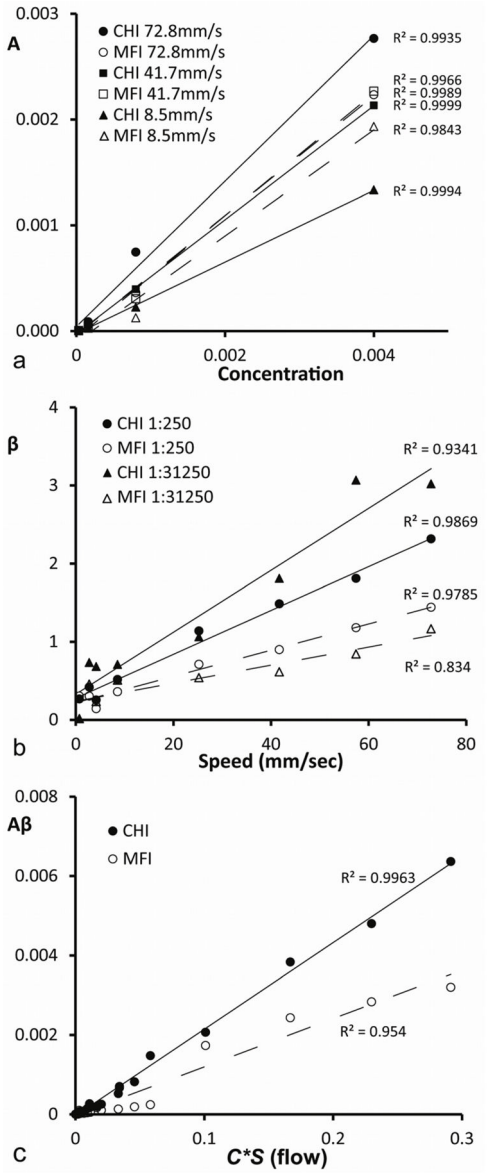

Fig. 3.

Summary of flow phantom validation experiments. Scatter plots show correlations between A and *C* at different contrast infusion speeds (a), correlations between β and *S* at different bubble concentrations (b), and the correlations between Aβ and *C*S* with lumped data (c).

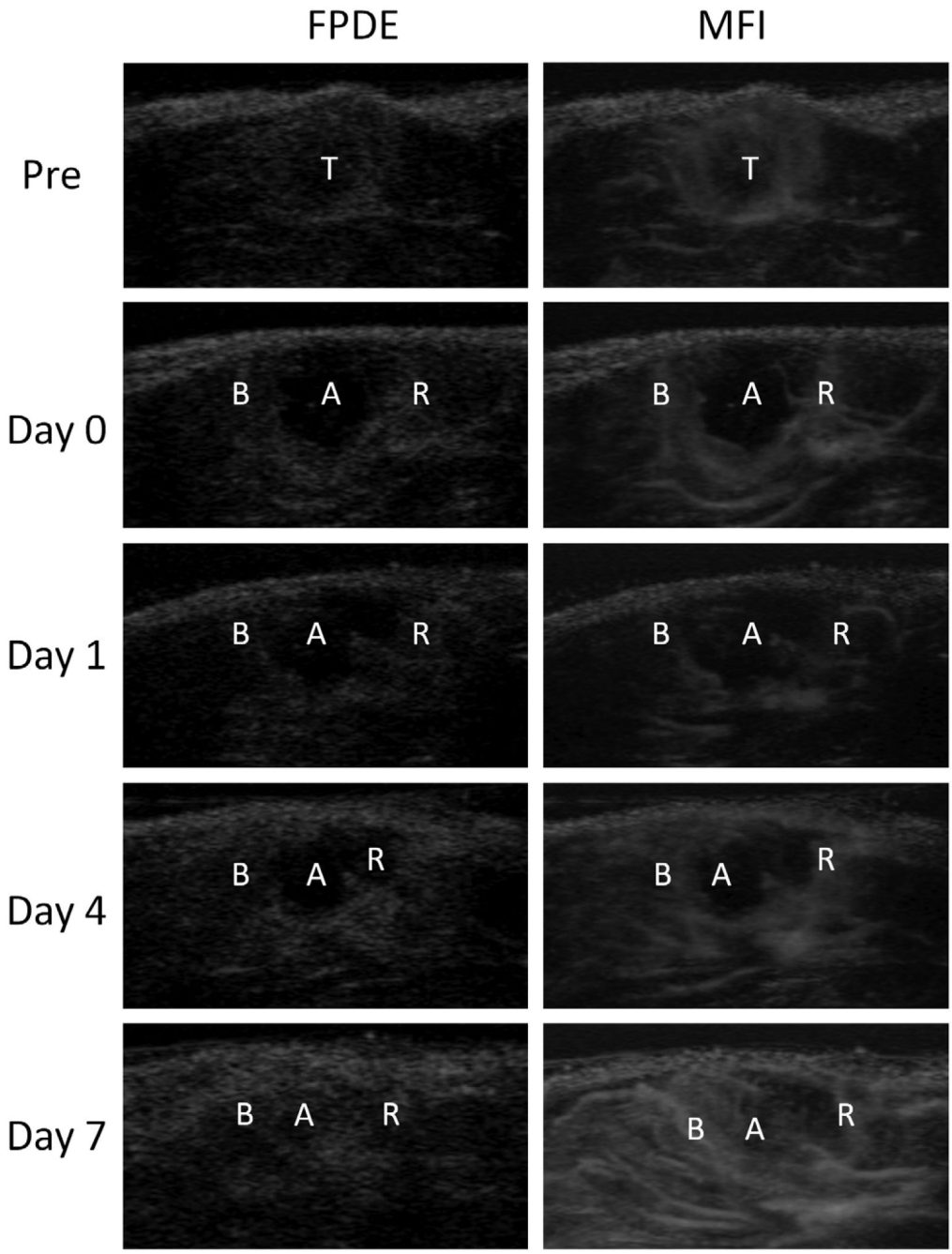

Fig. 4.

Representative FPDE and MFI images of a tumor before RF ablation, and days 0, 1, 4, 7 after RF ablation. T, untreated tumor; A, RF ablation zone; B, BPE; R, residual tumor.

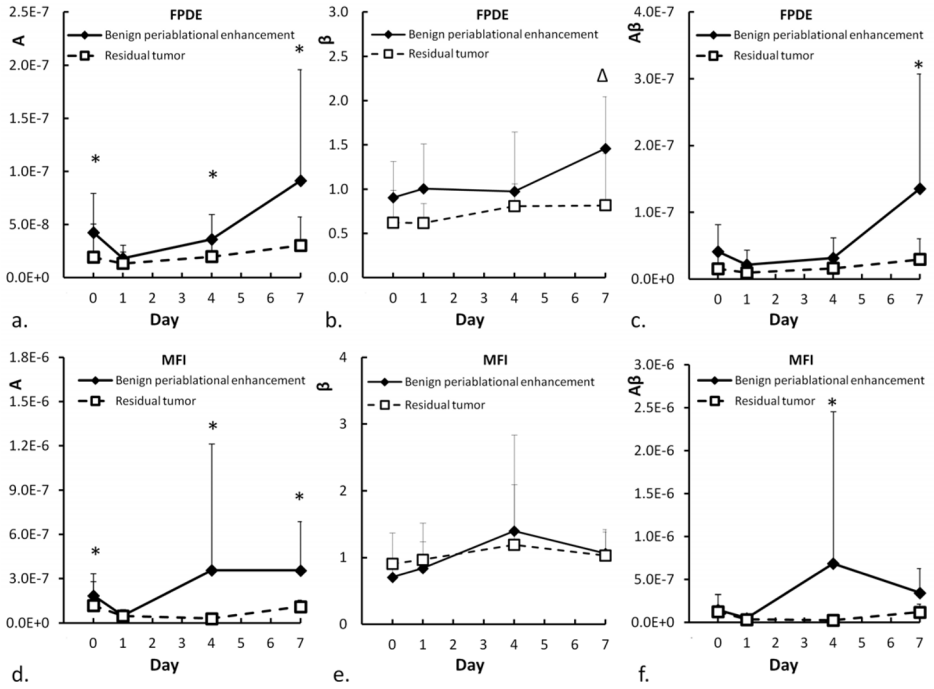

Fig. 5.

Scatter plots showing the changes of A, β, and Aβ values in BPE and residual tumor of first pass perfusion (a, b, c) and replenishing microflow perfusion (d, e, f). * Wilcoxon Signed-Rank test, $P < 0.05$, $^{\Delta}P = 0.05$.

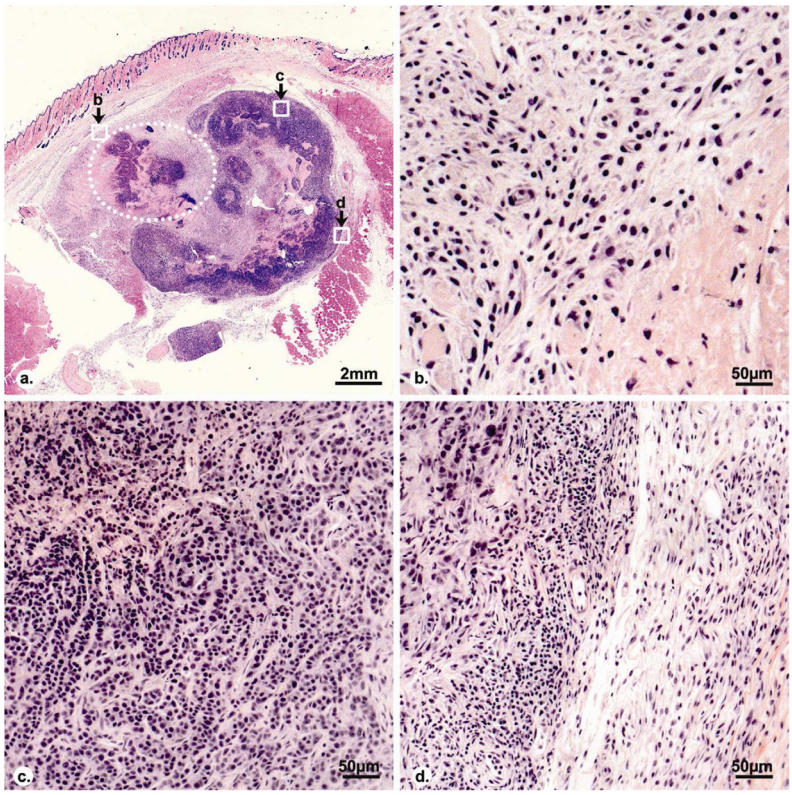

Fig. 6.

Histopathologic images (H&E stain) of a representative tumor on day 7 after RF ablation. A coagulation region (dotted line) locates at the side of the tumor. Central necrosis is visible in the residual viable tumor. Graphs b, c, d show the inflammatory rim of ablated region, residual viable tumor and residual tumor rim, respectively. Granulation tissue with inflammatory vessels is shown in inflammatory rim of ablated region (b). Extensive lymphocyte infiltrate is visible in the fibrous capsule of residual viable tumor with small vessels (d).

Table 1

Comparison of the fitting parameters of time-signal-intensity-curve of FPDE in BPE and residual tumor following RF ablation.

Day	BPE	Residual tumor	W	p
A				
0	4.25E-8 ± 3.71E-8	1.93E-8 ± 3.13E-8	30	0.025
1	1.83E-8 ± 1.24E-8	1.35E-8 ± 1.07E-8	12	> 0.05
4	3.61E-8 ± 2.34E-8	1.98E-8 ± 1.37E-8	28	<0.05
7	9.13E-8 ± 1.05E-7	3.04E-8 ± 2.7E-8	30	0.025
β				
0	0.91 ± 0.41	0.62 ± 0.37	16	>0.05
1	1.01 ± 0.51	0.62 ± 0.22	22	>0.05
4	0.97 ± 0.67	0.81 ± 0.25	12	>0.05
7	1.46 ± 0.58	0.82 ± 0.59	26	0.05
Aβ				
0	4.13E-8 ± 4.03E-8	1.54E-8 ± 2.81E-8	24	>0.05
1	2.16E-8 ± 2.19E-8	9.63E-9 ± 9.88E-9	10	>0.05
4	3.14E-8 ± 3.06E-8	1.61E-8 ± 1.19E-8	10	>0.05
7	1.35E-7 ± 1.72E-7	2.94E-8 ± 3.11E-8	32	<0.025

Wilcoxon Signed-Rank test, one-tail.

Table 2

Comparison of the fitting parameters of time-signal-intensity-curve of MFI in BPE and residual tumor following RF ablation.

Day	BPE	Residual tumor	W	p
A				
0	1.86E-7±1.48E-7	1.19E-7±1.61E-7	30	0.025
1	5.05E-8 ± 3.63E-8	4.76E-8 ± 4.41E-8	6	>0.05
4	3.58E-7 ± 8.57E-7	3.06E-8 ± 2.37E-8	36	0.005
7	3.57E-7 ± 3.32E-7	1.11E-7 ± 4.37E-8	30	0.025
β				
0	0.71 ± 0.29	0.91 ± 0.46	−16	>0.05
1	0.84 ± 0.40	0.97 ± 0.55	−6	>0.05
4	1.40 ± 1.44	1.19 ± 0.90	0	>0.05
7	1.06 ± 0.35	1.03 ± 0.36	−6	>0.05
Aβ				
0	1.47E-7 ± 1.80E-7	1.27E-7 ± 2.01E-7	4	>0.05
1	5.00E-8 ± 5.56E-8	3.61E-8 ± 3.53E-8	10	>0.05
4	6.87E-7 ± 1.77E-6	2.76E-8 ± 2.00E-8	28	<0.05
7	3.45E-7 ± 2.85E-7	1.22E-7 ± 9.13E-8	24	>0.05

Wilcoxon Signed-Rank test, one-tail.